Structural and Mechanistic Investigation of Rubidium Ion Exchange in Potassium Zirconium Trisilicate

Christopher S. Fewox, Sharath R. Kirumakki, and Abraham Clearfield*

Department of Chemistry, Texas A&M University, P.O. Box 30012, College Station, Texas 77842-3012

Received August 3, 2006. Revised Manuscript Received October 25, 2006

Complete and intermediate incorporation of rubidium into the hydrothermally prepared mineral umbite has been accomplished by ion exchange. Potassium zirconium trisilicate, $K_2ZrSi_3O_9 \cdot H_2O$, is an open framework ion exchanger composed of polymeric chains of trisilicate groups linked by zirconium atoms. This arrangement creates a three-dimensional tunnel network. The exchangeable cations are found in two unique tunnels along the *c*-axis inside the framework. Site 1 is marked by a 12-membered ring and contains two cations. Site 2, a 16-membered ring, contains two cations and two water molecules. The parent compound, $K_2ZrSi_3O_9 \cdot H_2O$, was used to prepare compound **1**, $Rb_2ZrSi_3O_9 \cdot H_2O$, in which the original space group, $P2_12_12_1$, is conserved. Cell dimensions of $a = 10.4821(6)$ Å, $b = 13.3869(5)$ Å, and $c = 7.2974(3)$ Å were found for compound **1**. Analysis of Rb−O coordination shows average contact distance approaching the sum of the O^{2-} and Rb^+ ionic radii. Compound **2**, $K_{0.29}H_{0.1}Rb_{1.61}ZrSi_3O_9 \cdot H_2O$, shows that Rb^+ has completely substituted K^+ in site 2 and only partially in site 1. Upon structural analysis of ∼50% incorporation of Rb^+, $K_{0.9}H_{0.1}RbZrSi_3O_9 \cdot H_2O$ (**3**), and ∼22.5% incorporation, $K_{1.45}H_{0.1}Rb_{0.45}ZrSi_3O_9 \cdot H_2O$ (**4**), it becomes apparent that the mechanism of exchange involves population of site 2 first. Further investigation of the mechanism of exchange through examination of the exchange kinetics has shown a plausible intermediate hydrolysis step occurs where K^+ is replaced by H^+ and subsequently H^+ exchanges with Rb^+.

Introduction

One of the significant problems facing the U.S. today is the legacy of our nuclear endeavors. Spent fuel from nuclear reactors, waste from weapons production, and medical and research waste must all be disposed of safely and effectively. Nuclear waste sites such as those in Hanford, Washington, and Savannah River, South Carolina, maintain high-level waste interim storage facilities that are operating beyond their original lifetime designs. Approximately 2400 million curies are spread over several sites around the country.[1] Permanent disposal of these waste streams is a national goal and a point of research important to all. Sorbents, porous materials, and ion exchange materials will play a significant role in the clean up process. By separating high activity isotopes and other actinides, waste can be segregated and processed according to contamination threat, isotope half-life, and activity.

The applications of porous materials span catalysis, gas adsorption and separation,[2] nuclear waste remediation, and ion exchange. For ion exchange and waste remediation, a wide variety of porous materials have been tested, from natural clays and layered materials to synthetic zeolites, metal oxides, and silicates.[3−11] For use as an ion exchanger in waste streams, these materials perform well in that, unlike some of their organic counterparts, they stand up to the high levels of radiation and are thermally and chemically stable in highly basic or acidic conditions. The selectivity of these materials for specific cations in highly competitive media is the subject of global research endeavors.

Efforts to increase selectivity and separate complex mixtures of radioactive cations from the before mentioned waste facilities have directed research toward new silicates, which incorporate octahedral metals.[12−14] Compounds have been developed and tested with zeolite-type pores of smaller dimensions and unique cavities to increase selectivity.[15,16] To better understand the selectivity of these materials, structural and mechanistic analysis of the ion exchange

* Corresponding author. Tel.: (979) 845-2936. Fax: (979) 845-2370. E-mail: clearfield@mail.chem.tamu.edu.

(1) Crowley, K. D.; Ahearne, J. F. *Am. Sci.* **2002**, *90*, 514.
(2) Sebastian, V.; Lin, Z.; Rocha, J.; Tellez, C.; Santamarıa, J.; Coronas, J. *Chem. Commun.* **2005**, *24*, 3036.
(3) Al-Attar, L.; Dyer, A. *J. Radioanal. Nucl. Chem.* **2001**, *247*, 121.
(4) Kodama, T.; Nagai, S.; Hasegawa, K.; Shimizu, K.; Komarneni, S. *Sep. Sci. Technol.* **2002**, *37*, 1927.
(5) Dyer, A.; Pillinger, M.; Harjula, R.; Amin, S. *J. Mater. Chem.* **2000**, *10*, 1867.
(6) Al-Attar, L.; Dyer, A.; Harjula, R. *J. Radioanal. Nucl. Chem.* **2004**, *260*, 199.
(7) Al-Attar, L.; Dyer, A.; Harjula, R. *J. Mater. Chem.* **2003**, *13*, 2963.
(8) Chorover, J.; Choi, S.; Amistadi, M. K.; Karthikyan, K. G.; Crosson, G.; Mueller, K. *Environ. Sci. Technol.* **2003**, *37*, 2200.
(9) Lee, Y.; Kim, S.-J.; Schoonen, M. A. A.; Parise, J. B. *Chem. Mater.* **2000**, *12*, 1597.
(10) Wang, X.; Liu, L.; Jacobson, A. J. *J. Am. Chem. Soc.* **2002**, *124*, 7812.
(11) Yang, X.; Makita, Y.; Hosokawa, J.; Sakane, K.; Ooi, K. *Chem. Mater.* **2005**, *17*, 5420.
(12) Behrens, E. A.; Poojary, D. M.; Clearfield, A. *Chem. Mater.* **1996**, *8*, 1236.
(13) Poojary, D. M.; Cahill, R. A.; Clearfield, A. *Chem. Mater.* **1994**, *6*, 2364.
(14) Pertierra, P.; Salvadó, M. A.; Garcia-Granda, S.; Khainakov, S. A.; Garcia, J. R. *Thermochim. Acta* **2004**, *423*, 113.
(15) Zheng, Z.; Philip, C. V.; Anthony, R. G.; Krumhansl, J. L.; Trudell, D. E.; Miller, J. E. *Ind. Eng. Chem. Res.* **1996**, *35*, 4246.
(16) Tripathi, A.; Medvedev, D.; Nyman, M.; Clearfield, A. *Solid State Chem.* **2003**, *175*, 72.

10.1021/cm061835x CCC: $37.00
Published on Web 12/29/2006

phases has been closely scrutinized.[17,18] In some cases, alterations to the framework have led to a change in uptake of selected cations. The environment of the cation has shed light on the reasons for increased cation affinity such as increase in coordination number.[19]

Another class of silicates investigated for their ion exchange abilities has the topology of the mineral umbite and has been synthesized under hydrothermal conditions.[20−23] Potassium zirconium trisilicate, $K_2ZrSi_3O_9 \cdot H_2O$, is an open framework compound with three-dimensional zeolite-like tunnels. Its ion exchange phases with Na^+ and Cs^+ have been prepared and characterized.[24] It has been shown that, among the alkali cations, rubidium is preferred over the entire pH range.[25] The rubidium phase has not, however, been characterized.

It is the goal of this study to shed light on the affinity of zirconium trisilicate for rubidium through structural analysis of the ion exchanged forms and in depth examination of the possible ion exchange mechanism.

Experimental Section

Reagents. All reagents were of analytical grade purity (Aldrich) and were used without further purification. ^{86}Rb was procured from Perkin-Elmer.

Analytical Procedures and Instrumentation. Phase identification and structural data sets were collected using a Rigaku computer automated diffractometer and a Bruker-AXS D8 powder diffractometer. Thermal gravimetric analysis was conducted on a TA Instruments TGA Q 500 unit. A constant temperature ramp of 5 °C/min was applied while the sample was under 9:1 nitrogen to air volume ratio. Potassium analysis was performed on a Varian AA250 atomic absorption spectrometer under an acetylene nitrous oxide flame. Samples for AA analysis were prepared by digestion of solid in hydrofluoric acid. Titrations and pH measurements were conducted on a TitraLab TIM860 Titration Manager. Measurements of ^{86}Rb uptake were performed on a Wallac 1410 liquid scintillation counter.

Synthesis of $K_2ZrSi_3O_9 \cdot H_2O$ and Its Rubidium Ion Exchanged Phases. Potassium zirconium trisilicate was synthesized hydrothermally by modification of methods previously reported by Poojary et al.[24] 7.0 grams of silicic acid was dissolved in 45 mL of 4 M KOH and 10 mL of isopropanol. 13.5 mL of a 70% solution of zirconium isopropoxide in isopropanol was diluted with 10 mL of isopropanol and added dropwise to the previous solution. The mixture was divided in two and placed in a 100 mL steel Teflon lined autoclave. The reaction was carried out at 180 °C. After 5 days, a white precipitate was isolated by vacuum filtration and washed twice with 50 mL of distilled water. Anal. Calcd for $K_2ZrSi_3O_9 \cdot H_2O$: Zr, 21.93; Si, 20.24; K, 18.80. Found: Zr, 21.73; Si, 20.52; K, 19.03.

Ion Exchange. Rubidium exchanged compounds were derived from $K_2ZrSi_3O_9 \cdot H_2O$. Particles of ion exchanger were ground to a sieved size of 150 μm or less. At room temperature, compound **1** was shaken with 0.1 M RbCl at a volume to mass ratio of 500:1 (mL/g) for 24 h. The product was captured by vacuum filtration and rinsed lightly with distilled water. The dried powder was then shaken with a 0.1 M solution of RbCl containing 0.01 M RbOH for 48 h. The product was filtered and washed thoroughly with boiling methanol. Anal. Calcd for $Rb_2ZrSi_3O_9 \cdot H_2O$: Zr, 17.96; Si, 16.59; Rb, 33.65. Found: Zr, 17.67; Si, 16.88; Rb, 32.81.

Compound **2** was produced by shaking 0.1 g of ion exchanger in 50 mL of 0.01 M RbCl for 48 h. The product was filtered, washed lightly with water, and dried at 60 °C. Compounds **3** and **4** were obtained by shaking the potassium umbite for 24 h with stoichiometric amounts of a 0.01 M RbCl solution to give the desired levels of substitution.

X-ray Data Collection and Structural Refinement. For structural characterization of the rubidium exchanged phases, a Rigaku automated powder diffractometer was used to collect data sets. A flat stainless steel sample holder was used in a Bragg−Brentano geometry. Data for compound **1** were collected at room temperature, while 2θ ranged from 5° to 90°. The X-ray source consisted of a rotating anode with a copper target and graphite monochromator. Operating voltage and current were 40 kV and 150 ma, respectively. A step size of 0.03° was employed with a scan rate of 7 s per step.

For compound **2**, data were collected from 5° to 90° 2θ using the same count time, step size, and operating power. Compounds **3** and **4** were collected on a Bruker-AXS D8 powder diffractometer using a quartz sample holder. Data were collected between 9° and 90° 2θ. Cu Kα radiation with an average wavelength 1.542 Å was employed. Operating voltage and current were 40 kV and 40 ma. Step size and scan rate were 0.02° and 10 s, respectively.

Powder patterns were indexed using the PowderX program suite.[26] Profile function fitting and Reitveld refinement were accomplished using the GSAS program suite. The LeBail method was used for extraction of structure factor amplitudes.[27,28] No corrections were made for absorption, and neutral atom scattering factors were used as stored in GSAS. No attempt was made to model preferred orientation.

Structural refinement was initiated by utilizing the coordinates of the framework atoms, as given by the original potassium zirconium trisilicate, as a starting model.[24] Contact distance constraints were applied for Si−O, Zr−O, and O−O contacts. The zirconium position was first refined and subsequently each trisilicate group. After initial refinement of atomic positions, Fourier difference maps were constructed to reveal the positions of the cations and water oxygen. These parameters were entered, and the framework positions were again refined without including the positions of the cations or water. Subsequently the cation and water positions were refined while holding the framework atom positions constant. This back and forth approach was continued until the shift in atomic position was minimal and the least-squares refinement converged rapidly. Together, cation, water oxygen, and framework positions were then refined.

(17) Larentzos, J. P.; Clearfield, A.; Tripathi, A.; Maginn, E. J. *J. Phys. Chem. B* **2004**, *108*, 17560.
(18) Dmitri, G.; Medvedev, D. G.; Tripathi, A.; Clearfield, A.; Celestian, A. J.; Parise, J. B.; Hanson, J. *Chem. Mater.* **2004**, *16*, 3659.
(19) Tripathi, A.; Dmitri, G.; Medvedev, D. G.; Delgado, J.; Clearfield, A. *J. Solid State Chem.* **2004**, *177*, 2903.
(20) Ilyushin, G. D.; Pudovkina, Z. V.; Voronkov, A. A.; Khomyakov, A. P.; Ilyukhin, V. V.; Pyatenko, A. *Sov. Phys. Dokl.* **1981**, *26*, 267.
(21) Ferreira, A.; Lin, Z.; Rocha, J.; Morais, C. M.; Lopes, M.; Fernandez, C. *Inorg. Chem.* **2001**, *40*, 3330.
(22) Bortun, A. I.; Bortun, L. N.; Poojary, D. M.; Xiang, O.; Clearfield, A. *Chem. Mater.* **2000**, *12*, 294.
(23) Henshaw, D. E. *Miner. Mag.* **1955**, *30*, 585.
(24) Poojary, D. M.; Bortun, A. I.; Bortun, L. N.; Clearfield, A. *Inorg. Chem.* **1997**, *36*, 3072.
(25) Clearfield, A.; Bortun, A. I.; Bortun, L. N.; Poojary, D. M.; Khainakov, S. A. *J. Mol. Struct.* **1998**, *470*, 207.
(26) Dong, C. *J. Appl. Crystallogr.* **1999**, *32*, 838.
(27) Larson, A.; Dreele, R. B. *GSAS: Generalized Structure Analysis System*; LANSCE, Los Alamos National Laboratory, Los Alamos, NM; Copyright 1985−88 by the Regents of the University of California.
(28) Le Bail, A.; Duroy, H.; Fourquet, J. L. *Mater. Res. Bull.* **1988**, *23*, 4467.

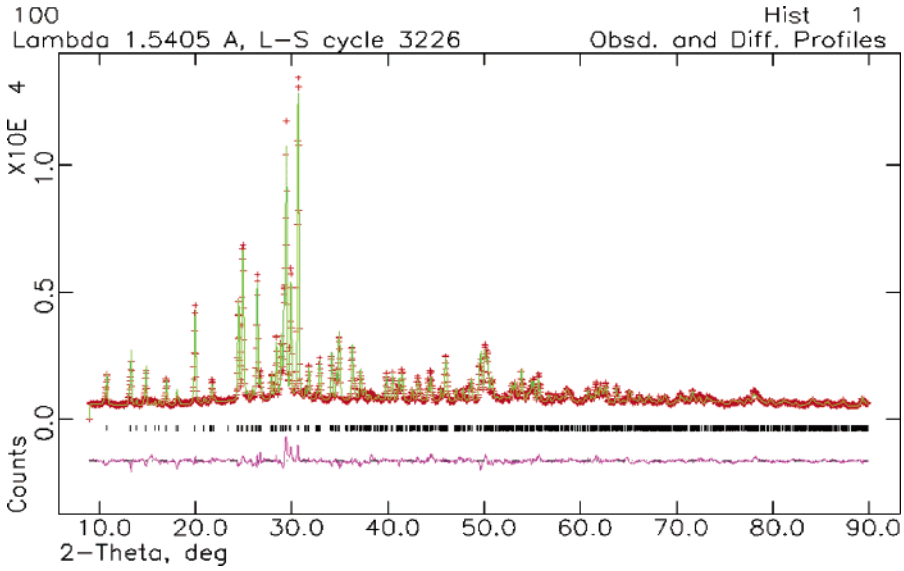

Figure 1. Observed (+) and calculated (−) profiles for final Reitveld refinement. Difference plot is shown in the bottom as the pink line. Reflections are marked by the black bars.

Table 1. Crystallographic Data for the Zirconium Trisilicate Phases[a]

	1	2	3	4
fw	508.43	486.38	457.30	432.67
space group	$P2_12_12_1$	$P2_12_12_1$	$P2_12_12_1$	$P2_12_12_1$
a (Å)	10.4782(7)	10.4575(5)	10.4029(7)	10.3591(6)
b (Å)	13.3831(7)	13.3712(5)	13.3484(8)	13.3296(7)
c (Å)	7.2940(5)	7.2861(3)	7.2591(5)	7.2315(4)
V (Å^3)	1022.84(14)	1018.81(8)	1008.01(14)	998.54(12)
Z	4	4	4	4
D_{calc} (g/cm^3)	3.288	3.258	2.995	2.860
no. of reflections	1021	1017	1008	1000
R_{wp}	0.0944	0.0976	0.1328	0.116
R_p	0.0694	0.0720	0.1052	0.0914

[a] Formulas: (**1**) $Rb_2ZrSi_3O_9{\cdot}H_2O$; (**2**) $K_{0.29}H_{0.1}Rb_{1.61}ZrSi_3O_9{\cdot}H_2O$; (**3**) $K_{0.9}H_{0.1}RbZrSi_3O_9{\cdot}H_2O$; (**4**) $K_{1.45}H_{0.1}Rb_{0.45}ZrSi_3O_9{\cdot}H_2O$.

During refinement of the atomic positions the weight applied to soft constraints was slowly reduced to a minimum where bond geometry was consistent and chemically meaningful. Isotropic thermal factors for zirconium, each cation position, and water oxygen were then refined, keeping silicon and oxygen factors fixed. No attempt was made to describe the water hydrogen positions.

For compound **1**, 1021 independent reflections were found in the 2θ range of 5−90°. Final refinement statistics show an R_{wp} of 0.0944 and an R_p of 0.0694. Systematic absences were consistent with the orthorhombic space group $P2_12_12_1$. Compound **1** displays unit cell dimensions of dimensions of a = 10.4821(6) Å, b = 13.3869(5) Å, and c = 7.2974(3) Å. The final refinement difference plot is shown in Figure 1. Crystallographic data are given in Table 1, and atomic coordinates and isotropic thermal factors for **1** are summarized in Table 2.

Ion Exchange Kinetics. Experiments were carried out under infinite solution volume conditions as specified by Helfferich.[29] Vigorous stirring was employed to ensure particle diffusion controlled kinetics and not film diffusion. The rate of Rb^+ uptake was measured by tracing a 0.01 M RbCl solution with enough ^{86}Rb to yield a count rate of ~50000 counts per min. A total of 0.4 g of ion exchanger was added to 200 mL of this solution under vigorous stirring. 1.0 mL aliquots were taken at designated times and filtered through a Millipore 0.22 μm syringe filter tip. The solution was then shaken with 18 mL of scintillation cocktail, and the amount of ^{86}Rb was measured on a Wallac 1410 liquid scintillation counter. Diffusion coefficients for the hydrolysis steps for $K_2ZrSi_3O_9{\cdot}H_2O$ and $Rb_2ZrSi_3O_9{\cdot}H_2O$ were measured on a TitraLab TIM860 Titration Manager. To 50 mL of distilled water adjusted to a pH of 7.0 was added 0.1 g of ion exchanger under stirring. Values of pH versus time were recorded and related to the Vermeulen approximation as seen in the Results.

(29) Helfferich, F. *Ion Exchange*; McGraw-Hill: New York, 1962.

Table 2. Positional and Thermal Parameters for $Rb_2ZrSi_3O_9{\cdot}H_2O$

	x	y	z	U_{iso}
Zr1	0.4432(7)	0.2117(5)	0.2558(13)	0.0315(29)
Si2	0.1656(13)	0.1772(12)	0.0184(19)	0.0800
Si3	0.0377(12)	0.0484(8)	0.7366(24)	0.0800
Si4	0.6448(13)	0.3291(12)	0.5641(20)	0.0800
O5	0.4237(16)	0.3657(8)	0.251(5)	0.0400
O6	0.3196(14)	0.2006(21)	0.0438(24)	0.0400
O7	0.5092(16)	0.0684(7)	0.252(4)	0.0400
O8	0.5643(19)	0.2368(17)	0.4665(28)	0.0400
O9	0.5899(16)	0.2278(17)	0.0796(29)	0.0400
O10	0.3001(14)	0.1924(21)	0.4374(25)	0.0400
O11	0.0962(16)	0.1598(15)	0.2206(20)	0.0400
O12	0.1152(22)	0.0636(15)	0.5406(25)	0.0400
O13	0.1455(21)	0.0729(16)	0.8985(27)	0.0400
Rb14	0.2044(10)	0.6294(7)	0.1906(18)	0.118(6)
Rb15	0.4316(7)	0.0813(5)	0.7311(15)	0.026(4)
Ow16	0.195(4)	0.4354(31)	0.105(5)	0.0150

Results

Structure of $Rb_2ZrSi_3O_9{\cdot}H_2O$ (1). The structure of the fully exchanged rubidium phase is analogous to that of the parent K^+ compound.[24] The zirconium atom links the infinite polymeric silicate chains to form the framework. Uptake of Rb results in expansion of the unit cell, increasing the cell

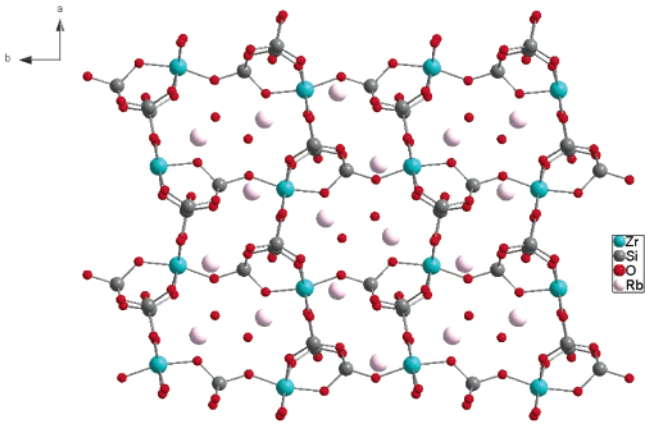

Figure 2. Ball and stick cartoon of compound **1** viewed down the *c*-axis. Rb14 is located in the 16-atom channel along with a water oxygen. Rb15 is seen in the 12-atom channel, which is unoccupied by water.

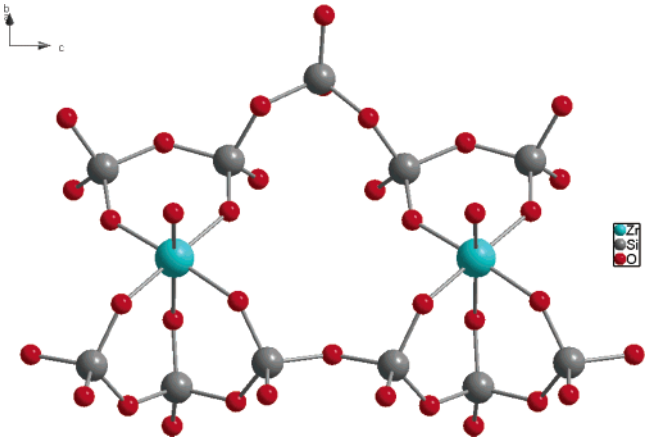

Figure 3. Ball and stick cartoon of the 14-atom channel linking sites 1 and 2. The view is approximately along the [$\bar{1}$10] plane.

volume by approximately 36 Å^3. The unit cell expansion takes place mainly along the *a*-axis, with an increase of approximately 0.2 Å. Further expansion of the unit cell is not as drastic along the *b*- and *c*-axes. The umbite-type structure contains a three-dimensional tunnel network similar to those found in zeolites. There are two independent cation exchange sites most easily defined by channels along the *c*-axis. As seen in Figure 2, site 1 is marked by a 16-atom ring formed by alternating silicate tetrahedra and zirconium−oxygen octahedra. Dimensions of this zeolite type pore are 5.7 Å × 7.2 Å. The site is occupied by two exchangeable cations and two water molecules. Site 2 is described by a 12-atom ring including two zirconium octahedra and four silicate tetrahedra. This site also contains two exchangeable cations, but no water. Site 2 is significantly smaller with dimensions of 3.2 Å × 6.4 Å. Sites 1 and 2 are connected by perpendicular tunnels approximately along the [$\bar{1}$10] diagonal. This connecting passageway between the two sites, depicted in Figure 3, is composed of a 14-atom ring approximately 4.4 Å × 7.0 Å. In essence, the simple motif of infinite silicate chains connected by zirconium octahedra builds the framework.

Selected bond distances for framework atoms for compounds **1**−**4** are shown in Table 3. Cation−oxygen distances for compounds **1**−**4** are summarized in Table 4. For compound **1** (Rb^+ content 100%), the rubidium environment

Table 3. Selected Framework Bond Distances (Å) for Compounds 1−4

bond	1	2	3	4
Zr1−O5	2.071(8)	2.059(8)	2.093(10)	2.097(9)
Zr1−O6	2.022(8)	2.030(10)	2.000(10)	2.015(10)
Zr1−O7	2.039(8)	2.039(8)	2.077(9)	2.045(8)
Zr1−O8	2.021(8)	2.023(10)	2.012(10)	2.007(9)
Zr1−O9	2.015(8)	2.017(10)	2.008(10)	1.993(10)
Zr1−O10	2.018(8)	2.011(10)	2.018(10)	2.022(10)
Si2−O6	1.654(8)	1.643(10)	1.651(6)	1.656(5)
Si2−O9	1.661(8)	1.660(11)	1.652(6)	1.662(5)
Si2−O11	1.661(8)	1.657(10)	1.647(6)	1.651(5)
Si2−O13	1.661(8)	1.660(11)	1.655(6)	1.658(5)
Si3−O5	1.660(8)	1.670(10)	1.653(6)	1.655(5)
Si3−O7	1.643(8)	1.647(9)	1.646(6)	1.650(5)
Si3−O12	1.657(8)	1.668(11)	1.656(6)	1.658(5)
Si3−O13	1.667(8)	1.677(11)	1.666(6)	1.664(5)
Si4−O8	1.657(8)	1.653(11)	1.656(6)	1.655(5)
Si4−O10	1.652(8)	1.641(9)	1.652(6)	1.655(5)
Si4−O11	1.658(8)	1.634(10)	1.649(6)	1.650(5)
Si4−O12	1.655(8)	1.641(10)	1.659(6)	1.656(5)

in ion exchange sites 1 and 2 shows Rb−O contact distances between 2.6 and 3.7 Å. In the large cavity (site 1), Rb14 is 10-coordinate, bonding to 8 framework oxygens (O5, O6, O7, O8, O8′, O9, O10, O11) and 2 water oxygens (Ow16, Ow16′). The closest cation−oxygen contact is with Ow16 at 2.67 Å. Rb15, located in the smaller cavity (site 2), is 11-coordinate and is bonded to 10 framework oxygens (O6, O7, O8, O9, O10, O11, O12, O12′, O13, O13′) and 1 water oxygen (Ow16). The close contact of Rb15 to a water oxygen is not seen in the parent compound where K^+ in the small tunnel shares no bond with water. While this contact is not as strong as the interaction of Rb14 with Ow16, it is still significant, and its distance, 3.016(42) Å, is within the sum of the ionic radii.

Structure of Partially Substituted Phases. Structure solutions for the partially substituted phases were carried out in the same fashion as for compound **1**. Compounds **2**, **3**, and **4** have identical framework compositions. The expansion of their unit cell volumes expresses the level of substitution, 1018, 1008, and 998 Å^3 for Rb^+ contents of 1.61, 1, and 0.45 mol, respectively, increasing from 987 Å^3 in the potassium phase. In all compounds where substitution was incomplete, hydrogen cations were observed in the structure. At equilibrium, the ion exchange solution displayed a pH of 10.65, indicating that, by charge balance, approximately 0.1 mol of H^+ must have remained in the exchanger. The largest difference in structure between compounds **2**, **3**, and **4** is the cation occupancy. For **2**, an excess of Rb^+ was allowed to come to exchange equilibrium with the K phase. This resulted in complete substitution of site 2 for Rb^+. In site 1, the occupancy was shown to be 0.29 K^+, 0.61 Rb^+, and 0.1 H^+. The coordination of Rb^+ cations in site 2 is the same as that of compound **1**. Average Rb−O contact distances are approximately 3.23 Å. An additional contact with O6 is shown at 2.999(17) Å. The Rb−Ow16 distance has increased from 3.016(42) to 3.311(42) Å.

To obtain the desired levels of substitution in compounds **3** and **4**, stoichiometric amounts of Rb^+ were exchanged at the same volume to mass ratio. Compound **4** shows an exchange of approximately 25% of Rb^+ for K^+ and has the formula $K_{0.45}H_{0.1}Rb_{0.45}ZrSi_3O_9{\cdot}H_2O$. The distribution of Rb^+ is uneven, and uptake is observed only in site 2. Final

Table 4. Cation−Oxygen Bond Distances (Å) for Compounds 1−4

compound	M14−O	distance	M15−O	distance
(**1**) $Rb_2ZrSi_3O_9 \cdot H_2O$	Rb14−O5	3.477(37)	Rb15−O6	3.021(26)
	Rb14−O6	3.446(26)	Rb15−O7	3.592(31)
	Rb14−O7	3.138(20)	Rb15−O8	3.161(23)
	Rb14−O8	3.042(23)	Rb15−O9	3.613(23)
	Rb14−O8′	3.716(23)	Rb15−O10	2.949(23)
	Rb14−O9	3.031(22)	Rb15−O11	3.241(21)
	Rb14−O10	3.017(27)	Rb15−O12	3.603(24)
	Rb14−O11	3.241(20)	Rb15−O12′	3.016(21)
	Rb14−Oω16	2.672(42)	Rb15−O13	3.239(23)
	Rb14−Oω16′	3.317(39)	Rb15−O13′	3.286(23)
			Rb15−Oω16	3.016(42)
(**2**) $K_{0.29}H_{0.1}Rb_{1.61}ZrSi_3O_9 \cdot H_2O$	M14−O5	3.426(23)	Rb15−O6	2.999(17)
	M14−O6	3.543(20)	Rb15−O7	3.664(25)
	M14−O7	3.145(16)	Rb15−O8	3.151(12)
	M14−O8	2.909(13)	Rb15−O9	3.474(12)
	M14−O8′	3.768(13)	Rb15−O10	2.991(16)
	M14−O9	3.137(13)	Rb15−O11	3.128(14)
	M14−O10	2.918(19)	Rb15−O12	3.701(12)
	M14−O11	3.191(14)	Rb15−O12′	2.954(12)
	M14−O12	3.720(14)	Rb15−O13	3.190(12)
	M14−Oω16	2.640(36)	Rb15−O13′	3.376(12)
	M14−Oω16′	3.162(38)	Rb15−Oω16	3.311(42)
(**3**) $K_{0.9}H_{0.1}RbZrSi_3O_9 \cdot H_2O$	M14−O5	3.369(31)	M15−O6	3.055(21)
	M14−O6	3.499(23)	M15−O7	3.376(22)
	M14−O7	3.121(20)	M15−O8	3.121(21)
	M14−O8	2.942(21)	M15−O9	3.67(2)
	M14−O8′	3.678(21)	M15−O10	2.847(20)
	M14−O9	3.005(20)	M15−O11	3.264(17)
	M14−O10	2.960(23)	M15−O12	3.675(19)
	M14-O11	3.312(19)	M15−O12′	2.953(19)
	M14−O12	3.660(21)	M15−O13	3.095(19)
	M14−Oω16	3.224(39)	M15−O13′	3.374(20)
	M14−Oω16′	2.566(38)	M15−Oω16	3.308(42)
(**4**) $K_{1.45}H_{0.1}Rb_{0.45}ZrSi_3O_9 \cdot H_2O$	K14−O5	3.285(31)	M15−O6	3.018(22)
	K14−O6	3.501(23)	M15−O7	3.431(25)
	K14−O7	3.089(22)	M15−O8	3.111(21)
	K14−O8	2.983(21)	M15−O10	2.832(21)
	K14−O8′	3.577(22)	M15−O11	3.231(19)
	K14−O9	2.935(21)	M15−O12	2.861(20)
	K14−O10	2.953(23)	M15−O13	3.069(19)
	K14−O11	3.320(21)	M15−O13′	3.354(21)
	K14−O12	3.603(22)	M15−Oω16	3.201(38)
	K14−Oω16	2.462(35)		
	K14−Oω16′	3.364(39)		

Reitveld refinement arrived at an occupancy in site 2 of 0.45 K^+, 0.45 Rb^+, and 0.1 H^+, while site 1 remains filled with K^+. K−O contacts in site 1 are between 2.5 and 3.6 Å. Four more K−O contacts are described here than in the original parent compound.[24] The average K−O distance has increased from 3.05 Å in the parent compound to 3.18 Å here in compound **4**. This can be attributed to the increase in the size of the unit cell.

Compound **3** is assigned the formula $K_{0.9}H_{0.1}RbZrSi_3O_9 \cdot H_2O$ as approximately 50% of K has been exchanged for Rb. Again, there is unequal distribution of Rb among the two exchange sites. Site 2 contains mostly Rb and has occupancy factors of 0.06 K^+, 0.84 Rb^+, and 0.1 H^+. Site 1 is now being populated by Rb cations either by direct exchange or through migration of the Rb ions in site 2 through the 14-atom channel. Site 1 occupancy factors are 0.86 K and 0.14 Rb. M−O contacts are similar to compound **4**. There are 11 M−O contacts in both sites. As in all other compounds reported here, there are two water contacts to the cation in site 1 and one M−Ow16 contact in site 2. The average contact distance is 3.21 Å in site 1 and 3.25 Å in site 2.

Kinetics. The kinetics of ion exchange reactions are limited by either diffusion through a film, or particle diffusion through pores or cavities of the exchanger. For particle diffusion control, derivations of the mathematical models that govern these processes begin with isotopic exchange. A variety of mathematical models can be employed, but all begin fundamentally with the description of ion flux. The flux of ion A in the ion exchanger is given by eq 1, where J_A is the flux, D is the coefficient of diffusion, and C_A is the concentration of ion A. The dependence of this flux, J_A, on time and concentration is given by Fick's second law (eq 2). Combination of eqs 1 and 2 yields eq 3. The solution to eq 3 yields C_A as a function of particle radius r and time t. Integration of this function yields eq 3a where fractional attainment of equilibrium, U, is a function of time t, particle radius r_o, and mass diffusion coefficient D_i.

$$J_A = -D \operatorname{grad} C_A \tag{1}$$

$$\frac{\partial C_A}{\partial t} = -\operatorname{div} J_A \tag{2}$$

$$\frac{\partial C_A}{\partial t} = D\left(\frac{\partial^2 C_A}{\partial r^2} + \frac{2}{r}\frac{\partial C_A}{\partial r}\right) \quad (3)$$

$$U(t) = 1 - \frac{6}{\pi^2}\sum_{n=1}^{\infty}\frac{1}{n^2}\exp\left(\frac{D_i t \pi^2 n^2}{r_o^{\,2}}\right) \quad (3a)$$

An important difference in mathematical modeling of ion exchange processes is the consideration of what Helfferich[29] refers to as electric coupling of ionic fluxes. It is this distinction that separates isotopic exchange from ion exchange. Distilled, this postulate states that as the faster ion diffuses an electric potential is set up, which accelerates diffusion of the slower ion while slowing diffusion of the faster ion. Thus, ion flux becomes dependent on the valence of the species in solution, and eq 1 is transformed into eq 4, where J_i is the transference of species i, φ is the electric potential, u_i is the electrochemical mobility, z_i is the valence of the ion, and C_i is the concentration.

$$J_{i\ \mathrm{electric}} = -u_i z_i C_i \ \mathrm{grad}\ \varphi \quad (4)$$

The electrochemical mobility u_i is defined as D_iF/RT, where D_i is the diffusion coefficient, F is the Faraday constant, R is the gas constant, and T is temperature in Kelvin. Incorporation of a flux term due purely to thermal diffusion, $J_{i\ \mathrm{diff}}$, gives the Nerst−Planck equation (eq 5).

$$J_i = J_{i\ \mathrm{diff}} + J_{i\ \mathrm{electric}} = -D_i\left(\mathrm{grad}\ C_i + z_i\frac{C_i F}{RT}\mathrm{grad}\ \varphi\right) \quad (5)$$

Under the assumption of electroneutrality and the absence of applied voltage to the system, the Nerst−Planck equation may be approximated in terms of D_i and r_o, which are the mass diffusion coefficient and the spherical radius of the ion exchange particle, respectively. A general form is shown in eq 6 and is expressed as a function of fractional attainment of exchange equilibrium $U(\tau)$, where τ is $D_A t/r_o^2$.

$$U(\tau) = (1 - \exp[\pi^2\{f(\alpha_1)\tau + f(\alpha_2)\tau^2 + f(\alpha_3)\tau^3\}])^{1/2} \quad (6)$$

Values of α are dependent on the valence ratios of the two exchanged ions z_A/z_B and are found tabulated by Helfferich.[29] An analysis of the practical application of mathematical models for isotopic exchange and ion exchange kinetics by Inglezakis and Grigoropoulou[30] shows that a simplified model known as Vermeulen's approximation, given in eq 7, may be used under a variety of conditions. In eq 7, $U(t)$ is the given fractional attainment of equilibrium, r_o is the size of the ion exchange particle in μm, t is time in seconds, and D_i is the mass particle diffusion coefficient and has units of $r_o^2\ t^{-1}$.

$$U(t) = \left[1 - \exp\left(\frac{D_i t \pi^2}{r_o^{\,2}}\right)\right]^{1/2} \quad (7)$$

According to Helfferich, application of the Vermeulen approximation gives less accurate results than that of the solution to eq 3a. However, in the domain of $F(t) \rightarrow 0.8$, as is the case with ion exchange data presented here, Helfferich suggests ignoring terms higher than first order, in which case eq 3a looks very similar to the Vermeulen approximation. Data were fit to eqs 3a, 7, and Paterson's approximation. In all cases, regression statistics favored the use of Vermeulen's approximation.

(30) Inglezakis, V. J.; Grigoropoulou, H. P. *J. Colloid Interface Sci.* **2001**, *234*, 434.

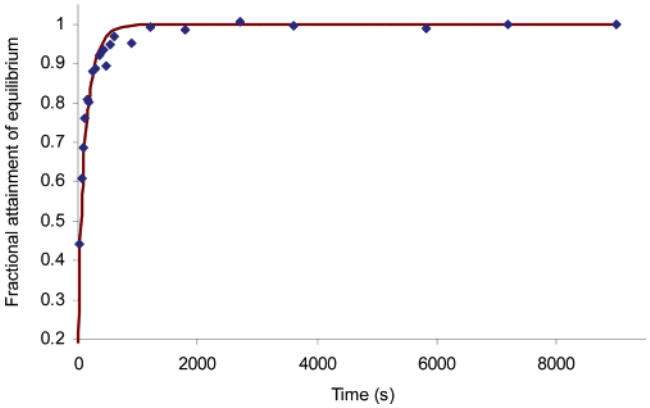

Figure 4. Plot of fractional attainment of equilibrium over time for the uptake of ^{86}Rb. Blue diamonds represent experimental points, while the maroon line represents the fit to Vermeulen's approximation.

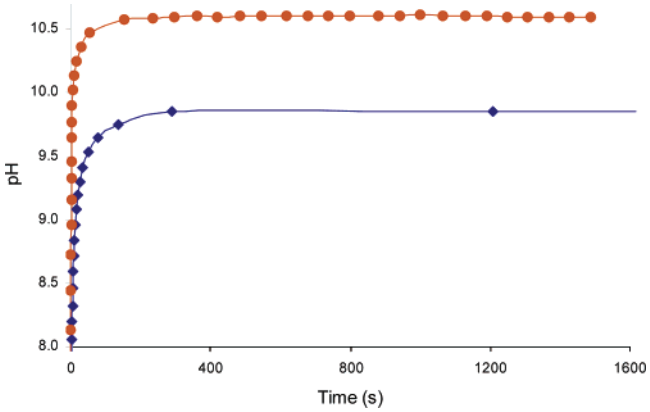

Figure 5. Plot of pH versus time for the hydrolysis of water upon addition of ion exchanger. Data in blue represent addition of $Rb_2ZrSi_3O_9{\cdot}H_2O$ to water, while the orange data represent addition of $K_2ZrSi_3O_9{\cdot}H_2O$ to water.

Results are summarized in Table 6. Experiments were carried out under infinite volume solution conditions where the concentration of K^+ in solution had no effect on attainment of equilibrium and no swelling of the exchanger occurred. A mass diffusion coefficient, D_i, of 3.4 $\mu m^2\ s^{-1}$ was observed for the ion exchange process of Rb exchange in $K_2ZrSi_3O_9{\cdot}H_2O$. Figure 4 shows the fractional attainment of equilibrium, which is proportional to uptake of ^{86}Rb as a function of time. Diffusion coefficients for the hydrolysis steps of both $K_2ZrSi_3O_9{\cdot}H_2O$ and $Rb_2ZrSi_3O_9{\cdot}H_2O$ were also measured as a function of fractional attainment of equilibrium. Figure 5 shows plots of pH as a function of time for the hydrolysis steps. Diffusion coefficients derived from these plots for Rb ↔ H and K ↔ H were 25.5 and 102.4 $\mu m^2\ s^{-1}$, respectively. A value of 75 μm was used for the particle radius r_o.

Infrared Spectrum. The infrared spectrum of compound **1** is shown in Figure 8. Bands of higher energy at approximately 740, 700, and 535 cm^{-1} have been reported as Zr−O stretches. Bands at 1040, 970, and 905 cm^{-1} are likely

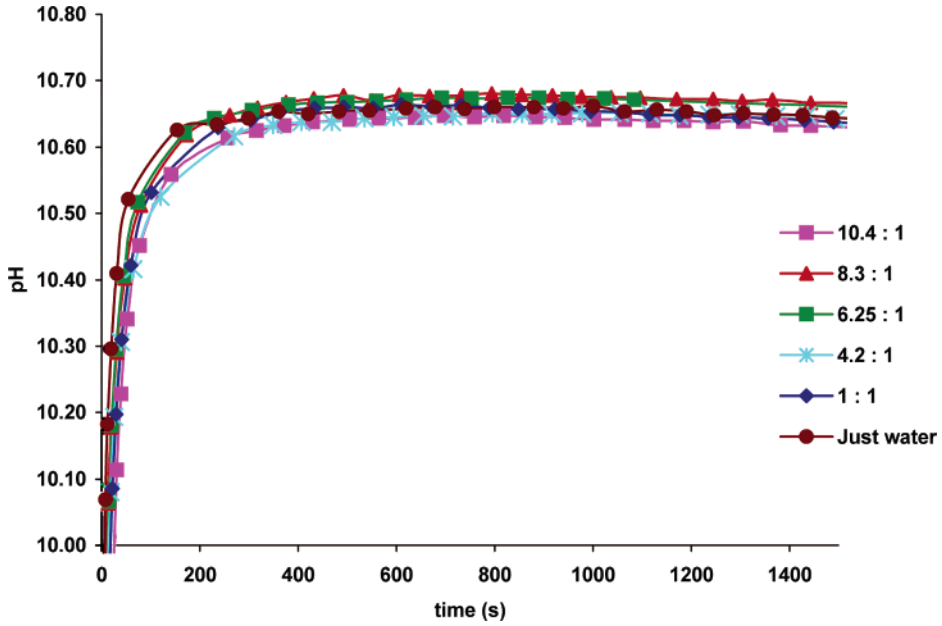

Figure 6. Plot of pH versus time for the ion exchange reaction of Rb with $K_2ZrSi_3O_9 \cdot H_2O$. Different Rb:K ratios are shown.

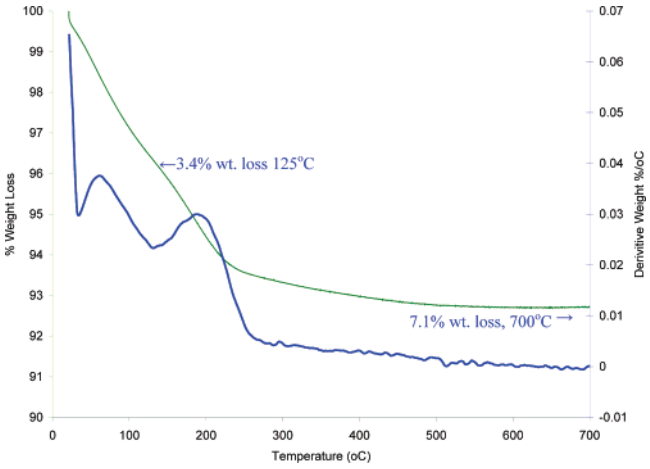

Figure 7. Thermal gravimetric curves of compound **1**. The green line represents % weight loss as a function of temperature. The blue line is the differential weight loss. An internal water loss of 3.7% was noticed, which accounts for 1 mole of water per mole of ion exchanger.

the symmetric and asymmetric stretches due to framework Si−O tetrahedra. It has also been reported that stretches in this region extend from those related to Si−O−Zr bonds.[31] The presence of water in site 1 can be confirmed by the bands located at 1640 cm^{-1} and at lower energy in the region of 3300 cm^{-1}. This is confirmed in the spectra reported for $K_2TiSi_3O_9 \cdot H_2O$.[22] Anomalous in this spectrum is the sharp absorbance at 1380 cm^{-1}. This can be attributed to the O−H bend of methanol, with which the sample was washed thoroughly.[32,33] Other modes for methanol such as the C−O stretch (1033 cm^{-1}) overlap with stronger absorbances of Si−O, while weaker C−H modes may also be masked in the areas of 1400−1650 cm^{-1}.

TGA. Thermogravimetric analysis of compound 1 indicated 3.4% weight loss at 125 °C (Figure 7). This loss is attributed to surface water. A total weight loss of 7.1% at 700 °C was observed. Therefore, 3.7% of the weight loss is due to lattice water. This number is slightly larger than the expected value of 3.54%. The discrepancy can be attributed to the presence of methanol as seen in the IR spectrum.

Discussion

Compounds **1**−**4** are isostructural with the mineral umbite, and all crystallize in the orthorhombic space group $P2_12_12_1$. The increase in unit cell volume for compounds **1**−**4** is directly related to the extent of exchange. The enlargement of the unit cell takes place mostly along the *a*-axis as the dimension increases from approximately 10.29(1) Å in the parent compound to 10.48(1) Å in compound **1**.

The selectivity of $M_2ZrSi_3O_9 \cdot H_2O$ and $M_2TiSi_3O_9 \cdot H_2O$ for alkali cations has previously been investigated.[25] The ability to collect specific ions is a direct relationship with the size of the channels and cavities they occupy. The affinity of zirconium trisilicate for each particular cation can now be correlated with the coordination environment of the cation. Table 5 shows the average M−O distances in sites 1 and 2 for the K^+, Na^+, and Rb^+ phases of zirconium trisilicate.[34] The coordination number of Rb in compound **1** is significantly higher than that for other cations in both ion exchange sites. Rb is 11-coordinate in site 1 and 11-coordinate in site 2; however, in the parent compound, K^+ is only 7-coordinate in both sites. This increase in coordination and the formation of additional M−O contacts can be said to account for the increase in selectivity for Rb. The Rb−O contact distances in **1** are closer to the sum of their ionic radii than that of K−O in the parent compound and Na−O in the sodium exchange phase. The Rb−O contacts in site 1 are approximately 0.12 Å larger than their ideal distance, while the disparities between those of K−O and Na−O are +0.19 and +0.62 Å, respectively. Rb−O contacts in site 2 are

(31) Dang, Z.; Anderson, B. G.; Amenomiya, Y.; Morrow, B. A. *J. Phys. Chem.* **1995**, *99*, 14437.
(32) Predoi-Cross, A.; Lees, R. M.; Johns, J. W. C. *J. Mol. Spectrosc.* **1998**, *191*, 348.
(33) Haase, F.; Sauer, J. *J. Am. Chem. Soc.* **1995**, *117*, 3780.
(34) Shannon, R. D.; Prewitt, C. T. *Acta Crystallogr.* **1969**, *B25*, 925.

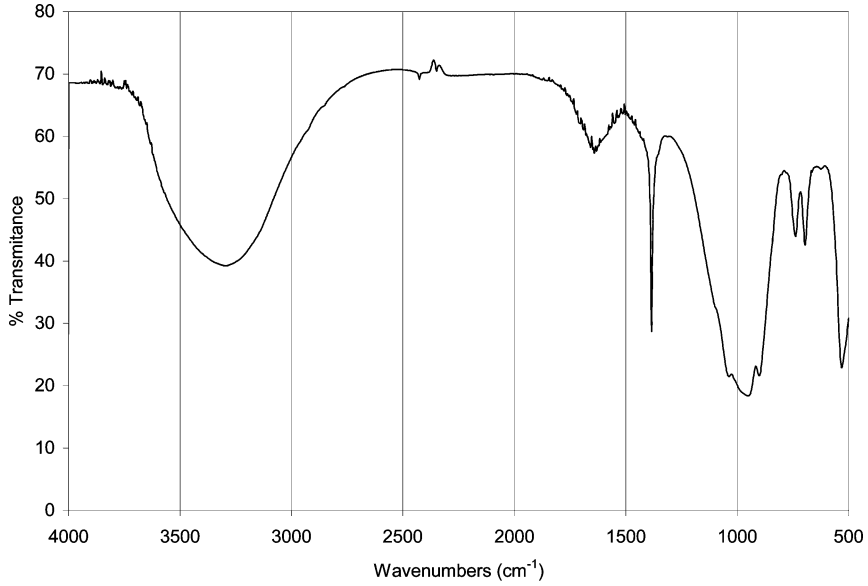

Figure 8. Infrared spectrum of compound **1**.

Table 5. Average Cation−Oxygen Distances Related to the Sum of Their Ionic Radii[24,31]

cation	coordination no. (site 1, site 2)	average M−O distance site 1 (Å)	average M−O distance site 2 (Å)	sum of ionic radii (Å)
Na	6, 9	3.04(2)	3.30(3)	2.42, 2.72
K	7, 7	3.05(1)	3.03(1)	2.86
Rb	10, 11	3.210(28)	3.243(25)	3.09

Table 6. Diffusion Coefficients Derived from Data Treatment with Vermeulen's Approximation

process	diffusion coefficient, D (μm^2 s^{-1})	Vermeulen regression statistics (R^2, χ^2/DoF)
K ↔ H	D_{KH} 102.4	0.976, 0.0018
Rb ↔ H	D_{RbH} 25.5	0.991, 0.00075
K ↔ H ↔ Rb	D_i 3.4	0.994, 0.00052

slightly longer than those of site 1. Average Rb−O contacts are 3.24 Å for site 2 in compound **1**, a difference of +0.15 Å from the ideal. For site 2, the differences between the sum of ionic radii and experimental M−O contacts are +0.19 Å for the K phase and +0.58 Å for the pure Na phase. Again, as the M−O contact distances approach those of the ideal, the affinity for that particular cation grows.

There are additional considerations to address before arriving at a pathway for potassium rubidium exchange. The diffusion coefficients measured for the separate processes occurring during exchange provide insight into the role of hydrolysis in this exchange mechanism. The mass diffusion coefficient given in Table 6 for the entire exchange process is 3.4 μm^2 s^{-1}. When the K-phase is placed in water, an equilibrium pH of approximately 10.65 is observed and the uptake of H^+ has been shown to have a diffusion coefficient of 102.4 μm^2 s^{-1}. Furthermore, it has been shown that this quantity, D_{KH}, is independent of Rb concentration (Figure 6). This quantity is 2 orders of magnitude greater than the mass diffusion coefficient and clearly indicates that it is the faster process. We can also see that the exchange of Rb^+ for H^+ is a slower process than exchange of K^+ for H^+. D_{RbH} was measured to be 25.5 μm^2 s^{-1}. Therefore, the rate-determining step in the incorporation of Rb into $K_2ZrSi_3O_9 \cdot H_2O$ is the exchange of H^+ for Rb^+ and not a direct exchange of potassium for rubidium.

The affinity of sites 1 and 2 for specific cations can also be distinguished on the basis of their coordination environment; however, the mobility of ions within the framework is a better method for describing the trends in site occupancy. As discussed in previous work, the shape of site 2 inhibits cation movement through the channel in the *c*-axis.[24] The distance between O12 and O13 effectively restricts the movement of cations along this direction; however, this does not prevent diffusion of cations between the two exchange sites. As previously described, a 14-atom channel links sites 1 and 2 approximately along the [$\bar{1}$10] plane.[24] Many mechanisms seem plausible; however, any mechanism must begin with loss of K^+ and must also account for the observed trends in site occupancy. A detailed description of the ion exchange process must also include the presence of H^+ in the mechanism. A possible pathway is discussed here that fits the experimental observations.

As previously stated, exchange must begin with the loss of K^+. Potassium cations may diffuse out into the solution through either the 14-atom tunnel or the 16-atom channel along the *c*-axis. If K^+ diffuses out through the large tunnel along the *c*-axis, a K^+ from site 2 may now move into site 1 via the 14-atom tunnel. A proton is then taken up in site 2 through either the 14-atom channel along the [$\bar{1}$10] plane or the 12-atom channel in the *c*-direction. As the exodus of K^+ continues through the 16-atom channel, Rb^+ replaces H^+ in site 2, which can diffuse out back into solution through the 12-atom channel along the *c*-direction. Remember, diffusion along the *c*-axis through the 12-atom channel is inhibited for larger cations by the encroachment of framework oxygens; however, this is not likely to limit the diffusion of H^+ because of its much smaller size. The fact that protons may diffuse through any and all channels makes

their replacement by Rb^+ faster than direct K^+ Rb^+ substitution and is in accordance with the kinetic data. Compound **2** shows that site 1 has been populated with Rb^+. Once site 2 is approximately 80% populated with Rb^+, diffusion of H^+ through site 2 along the *c*-axis becomes inhibited, and the exchange of cations through the framework must now occur almost entirely along the 16-atom channel.

Conclusions

Four compounds incorporating Rb into $K_2ZrSi_3O_9 \cdot H_2O$ have been synthesized by ion exchange, completing a series of alkali cation substituted zirconium trisilicates. Zirconium trisilicate shows maximum selectivity for Rb throughout the entire pH range. Among the fully substituted trisilicates, compound **1**, $Rb_2ZrSi_3O_9 \cdot H_2O$, shows M−O distances that are closest to their ideal distances, that being the sum of O^{2-} and Rb^+ ionic radii. It can now be said that, as the M−O distances approach those of the ideal, the affinity of zirconium trisilicate for a particular alkali cation increases.

Kinetic data have also been recorded and demonstrate a plausible part of the ion exchange mechanism. Upon addition of zirconium trisilicate to water, a pH increase is observed, indicating that protons are taken up through hydrolysis. The diffusion of H^+ into the trisilicate framework is 2 orders of magnitude faster than the mass diffusion coefficient measured for the overall exchange reaction of Rb^+ for K^+. This indicates that the exchange of K^+ for Rb^+ is much slower and the overall ion exchange process is actually exchange of K^+ by H^+ followed by replacement of H^+ with Rb^+.

Through structural analysis, it has been shown that site 2 is the first to be populated by Rb^+. The path of the cations as they diffuse in and out of the framework is still under investigation, and in-situ X-ray diffraction experiments have been planned to further elucidate the mechanism.

Acknowledgment. We acknowledge with thanks the U.S. Department of Energy, Environmental Management Science Program Grant No. De-FG07-01ER6300 with funds supplied through Westinghouse Savannah River Technology Center.

CM061835X